www.ietdl.org

Published in IET Power Electronics
Received on 9th July 2010
Revised on 16th September 2010
doi: 10.1049/iet-pel.2010.0231

ISSN 1755-4535

Analysis of a hybrid controlled three-phase grid-connected inverter with harmonics compensation in synchronous reference frame

D. Sha D. Wu X. Liao

School of Automation, Beijing Institute of Technology, 5 South Zhongguancun Street, Maidian District, Beijing 100081, People's Republic of China
E-mail: shadeshang@bit.edu.cn; shadeshang@gmail.com

Abstract: The power quality of three-phase grid-connected inverters has drawn attention with the increasing numbers of distributed generation systems. In order to effectively eliminate the harmonics in output currents, a hybrid system based on proportional–integral (PI) control and repetitive control (RC) implemented in the synchronous reference frame (SRF) is presented. Based on the reference frame transformation, the use of a repetitive controller is not for achieving fundamental reference current tracking but attaining the harmonics compensation, which is different from the RC designed in a static reference frame. In addition, analyses of the SRF-based hybrid controlled converter system, including stability constraints, harmonics rejection principles and the relationship between the PI controller and repetitive controller, are further developed in frequency domain and time domain. Finally, experimental results are demonstrated to validate the steady-state and dynamic performance of the proposed hybrid controlled system.

1 Introduction

Grid-connected technology is becoming a crucial issue in the distributed generation [1–3] to meet the stricter grid interconnection standards. According to the IEEE standards [4], the total harmonic distortion (THD) of the current injected to the grid should be lower than 5%. Since the power quality mainly depends on the output current, current-controlled (CC) voltage source inverters (VSI) [5, 6] are extensively used to interface the utility grid. Therefore different current control methods are proposed to achieve lower output harmonic distortions. As the predictive controller and hysteresis controller are well known for their fast response to eliminate low-order harmonics, they are used in current controllers to improve the output current quality [7, 8]. But these controllers require high sampling speed and still have little effect on eliminating higher harmonics. Another compensation method which has gained large popularity is the proportional resonant (PR) controller [9–11]. As the proportional–integral (PI) controller gets high loop gain at low frequencies to achieve zero steady-state error for direct current (DC) reference and disturbance, PR controller achieves high loop gain around the resonance frequency to reject the harmonic with the same frequency. However, since the distorted currents usually contain more than one order harmonics, it would be preferable to use many resonant compensators tuned at different harmonic frequencies cascaded together or nested in different rotating reference frames to achieve multiple harmonics compensation. Nevertheless, all the controllers mentioned above are unable to provide a large loop gain at the multiple harmonic frequencies to effectively compensate a wide bandwidth of harmonics; hence their compensation capability is therefore limited.

The repetitive control (RC) [12–14], based on internal model principle [15], is well known for its steady-state performance to control periodic components. From the frequency viewpoint, the RC presents large gain at the integral multiples of the fundamental frequency; consequently it offers a practical and simple solution for multiple harmonics compensation of converter systems [12]. As a result, many papers have been published to improve the performance of the converters with the RC scheme. In [16, 17], a robust RC scheme based on H_∞ control theory and linear phase compensated repetitive controller are presented to enhance the stability of the repetitive controlled system. A sliding mode repetitive control [18], odd-harmonic repetitive controller [19] and dual-mode repetitive controller [20] are proposed recently to improve the dynamic response of inverters. However, these repetitive controllers are all implemented in static reference frame, in which the repetitive controllers are not only used as a harmonic compensator but also as a controller to track the fundamental reference current. Therefore this kind of control scheme designed in static reference frame cannot be adopted under occasions needing fast response in terms of the slow dynamic property of the repetitive controller.

This paper presents a hybrid controlled scheme with RC-based harmonic compensator implemented in synchronous reference frame (SRF) for a three-phase grid-connected

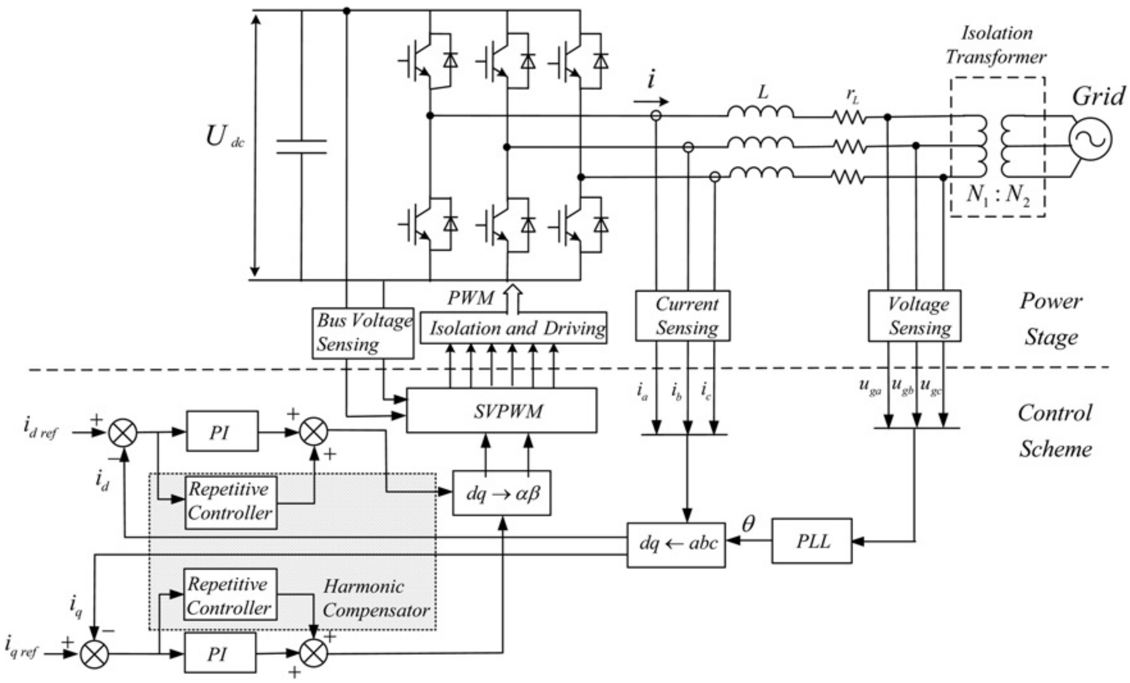

Fig. 1 *Three-phase grid-connected inverter with hybrid control scheme*

CC-VSI. As the fundamental alternating current (AC) components are transformed into DC components with the coordinate transformation, the fundamental current tracking is controlled by a conventional PI controller while grid harmonics are rejected by the RC harmonic compensator. In this paper, a detailed frequency analysis of the repetitive controlled harmonic compensator is presented. The correlation and different roles of the PI controller and repetitive controller in SRF, the selection of RC parameters and their contributions to the multiple harmonics compensation, the trade-off between the stability and compensation accuracy of the hybrid controlled system are further discussed in frequency domain and time domain. The system design procedure based on the frequency response analysis is given. Finally, the proposed control scheme is implemented in a 3 KVA three-phase grid-connected inverter to test the steady-state and dynamic performance of the system.

2 Modelling of the three-phase VSI in SRF

Fig. 1 shows a three-phase grid-connected CC-VSI incorporating a line-frequency transformer with the proposed hybrid control scheme. Space vector pulse width modulation technology is employed in the control system for its higher utilisation rate of the DC bus voltage. The three-phase inverter is connected to the grid through filtering inductors. As seen from Fig. 1, the model of VSI in static *abc* reference frame is

$$\frac{\mathrm{d}}{\mathrm{d}t}\begin{bmatrix} i_a(t) \\ i_b(t) \\ i_c(t) \end{bmatrix} = -\frac{r_L}{L}\begin{bmatrix} i_a(t) \\ i_b(t) \\ i_c(t) \end{bmatrix} + \frac{1}{L}\begin{bmatrix} u_a(t) - u_{ga}(t) \\ u_b(t) - u_{gb}(t) \\ u_c(t) - u_{gc}(t) \end{bmatrix} \tag{1}$$

where L and r_L are the filtering inductance and the parasitic resistance, i_a, i_b, i_c are the output currents of the inverter, u_a, u_b, u_c and u_{ga}, u_{gb}, u_{gc} are the line-to-neutral output voltages of the inverter and the grid side voltages, respectively.

The transformation matrix from static reference frame to SRF is

$$\boldsymbol{T} = \sqrt{\frac{2}{3}}\begin{bmatrix} \cos\,\omega t & \cos\left(\omega t - \frac{2\pi}{3}\right) & \cos\left(\omega t + \frac{2\pi}{3}\right) \\ -\sin\,\omega t & -\sin\left(\omega t - \frac{2\pi}{3}\right) & -\sin\left(\omega t + \frac{2\pi}{3}\right) \end{bmatrix} \tag{2}$$

By multiplying matrix $\boldsymbol{T}$ on both sides of (1), we have

$$\frac{\mathrm{d}}{\mathrm{d}t}\begin{bmatrix} i_d(t) \\ i_q(t) \end{bmatrix} = \begin{bmatrix} -\frac{r_L}{L} & \omega \\ -\omega & -\frac{r_L}{L} \end{bmatrix}\begin{bmatrix} i_d(t) \\ i_q(t) \end{bmatrix} + \frac{1}{L}\left(\begin{bmatrix} u_d(t) \\ u_q(t) \end{bmatrix} - \begin{bmatrix} u_{gd}(t) \\ u_{gq}(t) \end{bmatrix}\right) \tag{3}$$

where $\omega = 2\pi f$, f is the fundamental frequency of the grid voltage. Therefore taking the Laplace transformation of (3), the plant of VSI in each frame of SRF is as follows

$$G_p(s) = G_{dp}(s) = G_{qp}(s) = \frac{I(s)}{U(s)} = \frac{1}{Ls + r_L} \tag{4}$$

where $G_{dp}(s)$, $G_{qp}(s)$ denote the plant of the VSI in d–q reference frame, $I(s)$ represents the output current in d or q reference frame and $U(s)$ is defined as $U_m(s) - U_{gm}(s)$, $m = d, q$.

Since the SRF has the same rotating speed ω with the vector of the fundamental grid voltage, the AC variables with the fundamental frequency in three-phase static *abc* reference frame are transformed to be DC variables in SRF, and variables at harmonic frequencies in static *abc* reference frame are still AC variables with $\omega' = \omega_i - \omega$ as their angle frequencies in SRF (where ω_i is the angle frequency of the harmonic variables in *abc* reference frame). For example,

doi: 10.1049/iet-pel.2010.0231

the seventh positive sequence variables and the fifth negative sequence variables in *abc* reference frame are sixth positive sequence variables and sixth negative sequence variables, respectively, in SRF for $6\omega = 7\omega - \omega$ and $-6\omega = -5\omega - \omega$ [10]. In this case, we can see that the harmonics of grid voltages u_g in (1) (generally 5th, 7th, 11th, 13th harmonics for three-phase grid connected inverters) will cause corresponding harmonics in output currents. Therefore the good steady-state performance of the traditional PI controller in SRF will be weakened since the control variables are not absolute DC components under generalised grid conditions.

3 Control strategy for three-phase VSI in SRF

Fig. 2 shows the conventional control scheme in SRF, where $\omega L \cdot I_d(s)$ and $\omega L \cdot I_q(s)$ are decoupling factors and grid voltages can be viewed as disturbances $D_d(s)$, $D_q(s)$. Then, the tracking errors of each reference frame can be expressed as (see (5))

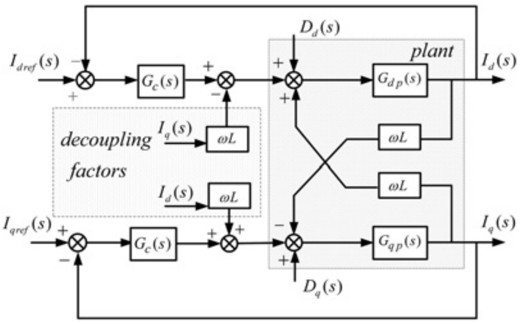

Fig. 2 *Conventional control scheme in d–q reference frame*

where $G_c(s)$ is a conventional PI type compensator, $I_{m\text{ref}}(s)|_{m=d,q}$ and $I_m(s)|_{m=d,q}$ are references and output currents of the VSI, respectively. According to the internal model principle, the zero-error steady-state tracking can be achieved only if the models of $I_{m\text{ref}}(s)|_{m=d,q}$ and $D_m(s)|_{m=d,q}$ are included in the model of $G_c(s)$. Because the references $I_{m\text{ref}}(s)|_{m=d,q}$ are DC variables in SRF, their models can be included in a PI controller of $G_c(s)$. The grid-side disturbance models $D_m(s)|_{m=d,q}$ are periodic AC variables and their models can be included in a repetitive controller.

Fig. 3 shows the hybrid control scheme with the repetitive controllers, where k_{rc} is the gain of the repetitive controller, Q is an integral coefficient that can be designed as a constant or a low-pass filter and $G_f(s)$ is a phase lead compensator [17]. As the disturbance model is 'learned' by the repetitive controller period by period, any disturbance model $D(s)$ with period T can be included in the controller for harmonics compensation of the output currents. The transfer function of the repetitive controller is

$$G_{\text{rc}}(s) = \frac{k_{\text{rc}} \times Qe^{-sT} \times G_f(s)}{1 - Qe^{-sT}} \tag{6}$$

With RC harmonic compensator, (5) can be revised as

$$\begin{cases} E'_d(s) = E_d(s) \times \dfrac{1 - Qe^{-sT}}{1 - (1 - k_{\text{rc}} \times G_f(s) \times H_d(s)) \times Qe^{-sT}} \\ E'_q(s) = E_q(s) \times \dfrac{1 - Qe^{-sT}}{1 - (1 - k_{\text{rc}} \times G_f(s) \times H_q(s)) \times Qe^{-sT}} \end{cases} \tag{7}$$

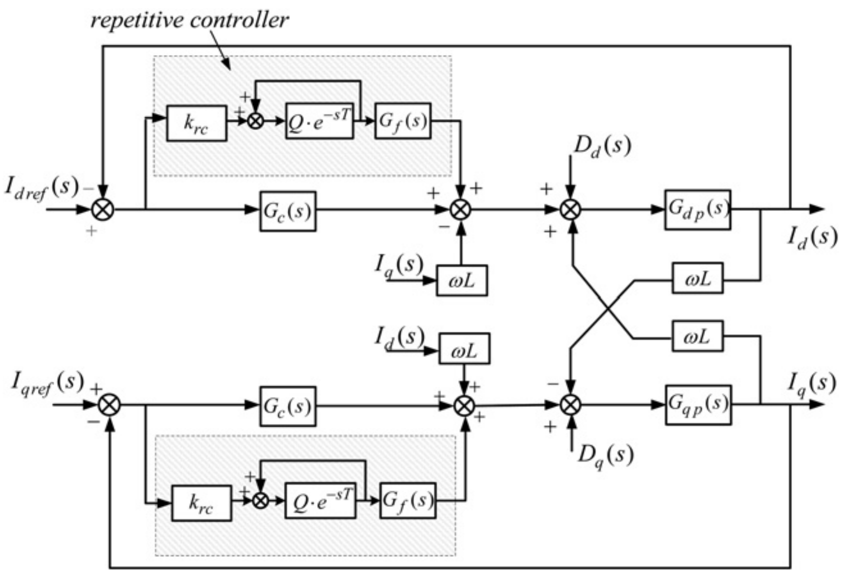

Fig. 3 *Three-phase VSI control scheme with RC-compensator*

$$\begin{cases} E_d(s) = I_{d\,\text{ref}}(s) - I_d(s) = \dfrac{1}{1 + G_c(s)G_{dp}(s)}[I_{d\,\text{ref}}(s) - G_{dp}(s)D_d(s)] \\ E_q(s) = I_{q\,\text{ref}}(s) - I_q(s) = \dfrac{1}{1 + G_c(s)G_{qp}(s)}[I_{d\,\text{ref}}(s) - G_{qp}(s)D_q(s)] \end{cases} \tag{5}$$

where $E'_d(s)$ and $E'_q(s)$ are the errors of the hybrid controlled system in $d-q$ reference frame, and $H_m(s)|_{m=d,q} = H(s) = \{(G_p(s))/(1+G_c(s)\cdot G_p(s))\}$ is the disturbance transfer function of Fig. 2.

4 Hybrid controlled system analysis

4.1 Stability analysis

For simplicity, the following discussion is only focused on d-frame and the same control strategy can also be applied to q-frame. From (7), the hybrid controlled system is stable if the poles of (5) are at the left side of the complex plane and the following condition is satisfied [12]

$$||1-(1-k_{\mathrm{rc}}\times G_f(s)\times H(s))\times Qe^{-sT}|| \neq 0, \quad s=j\omega \tag{8}$$

where $T=(1/f)$, $|e^{-sT}|=|e^{-j\omega T}|=1$. Equation (8) is guaranteed if the following condition is satisfied

$$|(1-k_{\mathrm{rc}}\times G_f(j\omega)\times H(j\omega))Q|<1 \tag{9}$$

where $Q\neq 0$, then we have [17]

$$|1-k_{\mathrm{rc}}\times G_f(j\omega)\times H(j\omega)|<\frac{1}{|Q|}, \quad \omega\in\left[0, \frac{\pi}{T_s}\right] \tag{10}$$

Fig. 4 shows the geometric explanation of (10) in complex plane. When $Q=1$, the stability condition (10) can be viewed equally as the vector $k_{\mathrm{rc}}G_f(j\omega)H(j\omega)$ ($\boldsymbol{OA}_1$, $\boldsymbol{OA}_2$) not exceeding the unit circle with C as its centre. Fig. 4 also indicates two features to ensure the stability of the hybrid controlled systems.

1. The phase of the vector $k_{\mathrm{rc}}G_f(j\omega)H(j\omega)$ should be within the range of $[-90°, 90°]$.
2. The magnitude of vector $k_{\mathrm{rc}}G_f(j\omega)H(j\omega)$ should be reduced when $\angle k_{\mathrm{rc}}G_f(j\omega)H(j\omega)\rightarrow \pm 90°$.

When $G_f(j\omega)=1$, it is difficult to design a PI controller that can ensure (10) and maintain a high dynamic performance for the VSI system both. In a practical design, the PI controller is usually first designed to achieve the best fundamental current tracking performance, and a

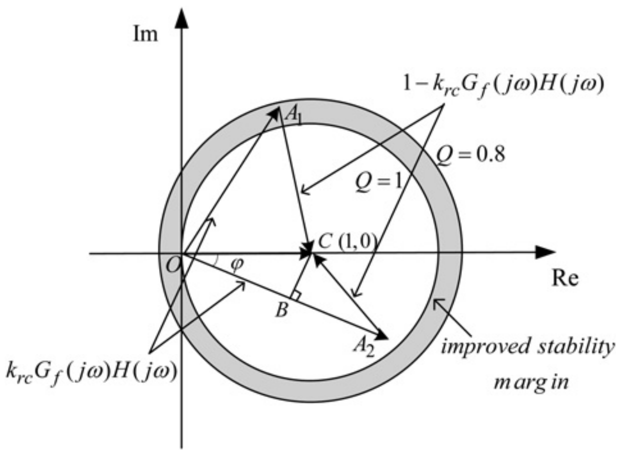

Fig. 4 *Illustration of stability condition for the hybrid controlled VSI system in complex plane*

compensator $G_f(j\omega)=e^{j\theta}$ is consequently designed to guarantee the stability of the VSI system when RC harmonic compensator is plugged in. On the other hand, the stability condition (b) will lead to a tough selection of the gain k_{rc} because a large k_{rc} will deteriorate the stability while small k_{rc} will slow the convergence rate of harmonics compensation.

Reducing the value of Q can simplify the selection of k_{rc}. The stability margin is improved with the left border of the circle enlarged when $\angle k_{\mathrm{rc}}G_f(j\omega)H(j\omega)\rightarrow \pm 90°$, and this can be seen from Fig. 4. For example, the vector $\boldsymbol{OA}_1$ exceeds the unit circle when $Q=1$. But the system becomes stable with $\boldsymbol{OA}_1$ staying in the larger circle when $Q=0.8$. With Q decreasing, k_{rc} can be selected larger and still maintain the stability of the system. However, the steady-state analysis shows that the harmonics cannot be fully rejected with $Q<1$.

To enhance the robustness and maintain $Q=1$, $G_f(j\omega)$ can be modified as $G_f(j\omega)=G_{f1}(j\omega)\cdot e^{j\theta}$, where $G_{f1}(j\omega)$ is a low-pass filter and $e^{j\theta}$ is the phase compensator. $G_{f1}(j\omega)$ is used to damp the magnitude of high frequencies when $\angle k_{\mathrm{rc}}G_f(j\omega)H(j\omega)\rightarrow \pm 90°$. When $Q=1$, the stability condition for k_{rc} in (10) can be obtained directly from the triangle $\boldsymbol{OBC}$ in Fig. 4

$$\begin{aligned} &|k_{\mathrm{rc}}G_f(j\omega)H(j\omega)|<2|\boldsymbol{OB}|=2|\boldsymbol{OC}|\cos\varphi \\ &\Leftrightarrow k_{\mathrm{rc}}<\frac{2\cos\varphi}{|G_f(j\omega)H(j\omega)|} \end{aligned} \tag{11}$$

where $\phi=\angle G_f(j\omega)H(j\omega)$.

4.2 Steady-state tracking error

Assuming the system is stable, (7) can be expressed by the Taylor progression as follows

$$\begin{aligned} E'(s) &= E(s)(1-Qe^{-sT})+E(s)[1-k_{\mathrm{rc}}G_f(s)H(s)] \\ &\quad \times Qe^{-sT}\times(1-Qe^{-sT}) \\ &\quad +\cdots+E(s)[1-k_{\mathrm{rc}}G_f(s)H(s)]^i \\ &\quad \times Q^i e^{-isT}(1-Qe^{-sT})+\cdots \end{aligned} \tag{12}$$

To observe the compensation effect of RC-harmonic compensator on the VSI system, the error of the hybrid controlled system can be further discussed in time domain by the inverse Laplace transform of (12). $e(t)$ can be written as

$$\begin{aligned} e(t) &= L^{-1}[E'(s)] = L^{-1}[E(s)(1-Qe^{-sT})] \\ &\quad + L^{-1}[E(s)[1-k_{\mathrm{rc}}G_f(s)H(s)] \\ &\quad \times Qe^{-sT}\times(1-Qe^{-sT})] \\ &\quad +\cdots+L^{-1}[E(s)[1-k_{\mathrm{rc}}G_f(s)H(s)]^i \\ &\quad \times Q^i e^{-isT}\times(1-Qe^{-sT})]+\cdots \\ &= e_0(t)-Qe_0(t-T)+e_1(t-T)-Qe_1(t-2T) \\ &\quad +\cdots+e_i(t-iT)-Qe_i(t-(i+1)T)+\cdots \end{aligned} \tag{13}$$

where $e_i(t)=L^{-1}\{E(s)[1-k_{\mathrm{rc}}G_f(s)H(s)]^iQ^i\}$, $i=0, 1, 2, \ldots$.

Assuming the error of the VSI system is caused by harmonics whose frequencies are the multiples of the fundamental frequency, we have $e_i(t-iT)=e_i(t-(i+1)T)$, where $i=0, 1, 2, \ldots, \infty$. Consequently

doi: 10.1049/iet-pel.2010.0231

(13) can be rewritten as

$$e(t) = \sum_{i=0}^{\infty} (1 - Q) \times e_i(t - iT) \tag{14}$$

The steady-state tracking error of the VSI system is presented as

$$\lim_{t\to\infty} e(t) = (1 - Q) \times \lim_{t\to\infty} \sum_{i=0}^{\infty} e_i(t - iT) \tag{15}$$

When $Q = 1$, the zero steady-state error tracking is achieved.

4.3 Dynamic response analysis

From (13), the error of the hybrid controlled VSI system at time t $e_i(t)$, $t \in [iT, (i+1)T]$ can be eliminated in the next period. If $k_{rc}G_f(s)H(s) = 1$ and $Q = 1$, the error will converge to zero in the second period and the dynamic response relies on the PI controller in the first period. In practice, $k_{rc}G_f(s)H(s) = 1$ is difficult to be satisfied, and the error $e_i(t)$, $t \in [iT,(i+1)T]$ is determined by $E(s)[1 - k_{rc}G_f(s)H(s)]^i$. We can see that the convergence rate is influenced by the parameters of the RC harmonic compensator and $E(s)$ acts as a common ratio of the convergence.

Note that the control of the VSI is implemented in SRF and the PI controller can achieve zero steady-state tracking error of the fundamental current. Therefore the error $e_0(t) = L^{-1}(E(s))$ is smaller than the error of the VSI implemented in static reference frame, which means the three-phase VSI controlled in SRF yields faster dynamic response and harmonic convergence rate theoretically.

5 System design and experimental results

5.1 Conventional PI controlled VSI in SRF

A three-phase VSI laboratory prototype is fabricated with the parameters listed in Table 1. Consequently, the plant transfer function of the three-phase VSI in each frame of SRF is

$$G_p(s) = \frac{1}{Ls + r_L} = \frac{1.67}{0.003s + 1} \tag{16}$$

The parameters of the PI controller can be preliminarily designed based on the system performance demand and then can be adjusted according to the experiment. The k_p and k_i are chosen as $k_p = 6$ and $k_i = 200$. Fig. 5 shows the Bode plot of the loop gain of PI controlled VSI in SRF, as seen, while after PI compensation, the compensated loop gain has a crossover frequency of 475 Hz and the phase margin is 95.1°.

Table 1 System parameters

DC-bus voltage U_{dc}	400 V
grid-side line-to-line voltage U_{grid} (rms)	380 V
fundamental frequency f	50 Hz
switching frequency f_s	5 kHz
filter inductance L	2 mH
resistance of the filtering inductor r_L	0.6 Ω
turns ratio of the line-frequency transformer N_1:N_2	1:2

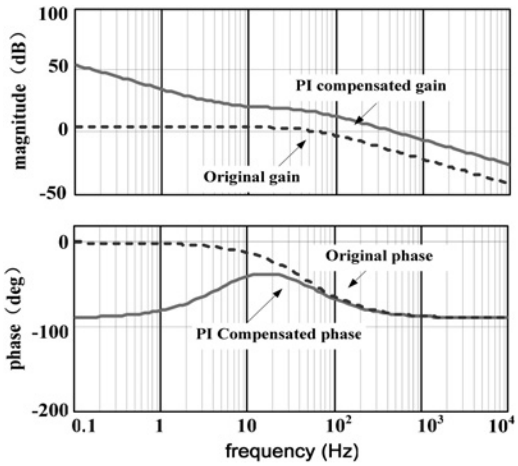

Fig. 5 *Bode plot of the loop gain of PI controlled VSI in SRF*

5.2 Design of the RC-harmonic compensator

Based on the disturbance transfer function $H(s)$ of the three-phase VSI without RC compensator, a phase compensator $e^{j\omega T c}$ [17] can be designed to meet the stability condition (1) mentioned in Section 4.1. For digital realisation, G_{rc} is designed as $G_{rc}(z) = k_{rc}\{(Qz^{-N})/(1 - Qz^{-N})\}G_f(z)$, $N = (T/T_s)$. And correspondingly T_c should be integral multiples of the sampling period T_s because the phase compensator is realised as z^n, $n = 0, 1, 2, \ldots$. Fig. 6 shows the Bode plot of $G_f(s)\cdot H(s)$ with different T_c. Table 2 shows the bandwidth of $G_f(s)\cdot H(s)$ with different leading compensation T_c. It can be seen from Table 2 that when $T_c = 0.0002s$, the system has the widest range to ensure the stability. Consequently, the range $0.05 < \cos\angle G_f(j\omega)H(j\omega) < 1$ can be obtained from Fig. 6. With (11), the gain of the repetitive controller should be selected as $0 < k_{rc} < 0.6$.

Fig. 7 shows the Bode plot of $G_{rc}(s)$ with $Q = 1$ and $k_{rc} = 0.5$ below 1 kHz. The diagram indicates that one RC

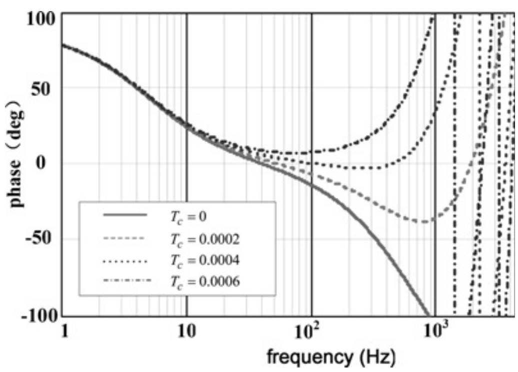

Fig. 6 *Bode plot of $G_f(s)\cdot H(s)$ with different T_c*

Table 2 Bandwidth of $G_f(s)\cdot H(s)$ for stability with different T_c

T_c, s	Bandwidth, Hz
0	[0, 720]
0.0002	[0, 3500]
0.0004	[0, 1600]
0.0006	[0, 900]

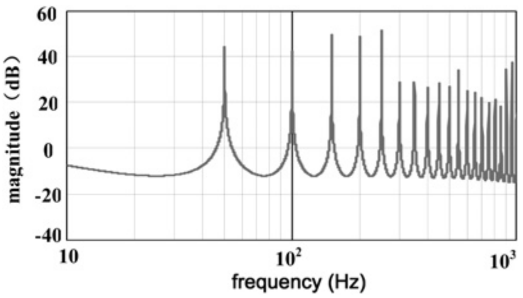

Fig. 7 *Bode plot of harmonic compensator $G_{rc}(s)$ with $Q = 1$ and $k_{rc} = 0.5$*

harmonic compensator can eliminate multiple harmonics because large magnitude for compensation is achieved at each harmonic frequency of $G_{\rm rc}(s)$.

To further discuss the harmonics rejection principles of the RC compensator, the influence of different parameters of $G_{\rm rc}(s)$ is compared in Bode plot of Fig. 8. It can be observed that the gain of RC compensator is determined by $k_{\rm rc}$, whereas the shape is governed by Q. The gain of $G_{\rm rc}(s)$ represents the harmonic convergence rate of the repetitive compensator, and the magnitudes of $G_{\rm rc}(s)$ at the harmonic frequencies denote the accuracy of harmonic compensation. Therefore the diagram illustrates that small $k_{\rm rc}$ will slow the compensation rate whereas the small Q will weaken the 'inherent' harmonic rejection in repetitive controlled harmonic compensator.

Fig. 9 shows the Bode plot of the system loop gain with and without the RC compensator. The parameters of $G_{\rm rc}(s)$ are selected as $Q = 1$ and $k_{\rm rc} = 0.5$. When the system is controlled with the RC compensator, it can be seen that the system loop gain achieves high magnitudes at harmonic frequencies compared to the system controlled without the RC compensator. From Fig. 9, it is also worth noting that the fundamental current tracking mainly depends on the PI controller when the SRF control strategy of the system is taken into consideration. This is the main difference between the conventional repetitive controllers implemented in static reference frame and the RC harmonic compensators in SRF, because the controller of the latter one mainly works for the harmonics instead of the fundamental components. The RC harmonic compensator also simplifies the controller design procedure compared to the selective harmonic compensators [21, 22], because one RC compensator provides a wide bandwidth of harmonic compensation as shown in Fig. 9. Besides, further improvement on the RC compensator in SRF can be

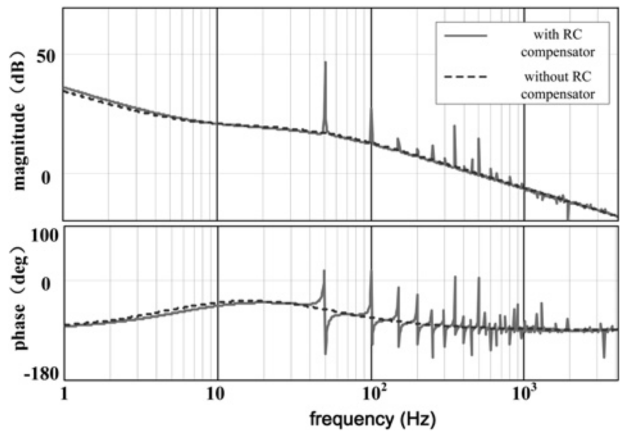

Fig. 9 *Bode plot of the system loop gain with and without RC compensator*

implemented by revising the T referring to the fundamental period as the period of harmonics to achieve selective harmonic compensation.

5.3 Experimental results

A 3 kW experimental prototype of three-phase VSI is fabricated to evaluate the performance with the proposed control scheme. The system parameters are described in Table 1 and the control is implemented by a TMS320F2407 digital signal processor with the parameters of the controllers selected in Table 3.

Fig. 10 shows the steady-state performance of three-phase VSI in SRF with and without RC compensator. In Figs. 10*a* and *b*, three-phase output currents are read from a external TLC7225 D/A converter. As seen, with and without RC harmonic compensator, the THD is 1.7 and 4.3%, respectively, and the measurement is implemented by Fluke 43B power harmonic analyser.

Figs. 10*c* and *d* show the single-phase output current i_a and transformed current in d frame i_d with and without the RC

Table 3 Parameters of the controllers

proportional gain $k_{\rm p}$ of PI controller	6
integral gain $k_{\rm i}$ of PI controller	200
gain of the RC compensator $k_{\rm rc}$	0.2
coefficient Q of the RC compensator	0.98
leading coefficient n in the phase compensator z^n	1

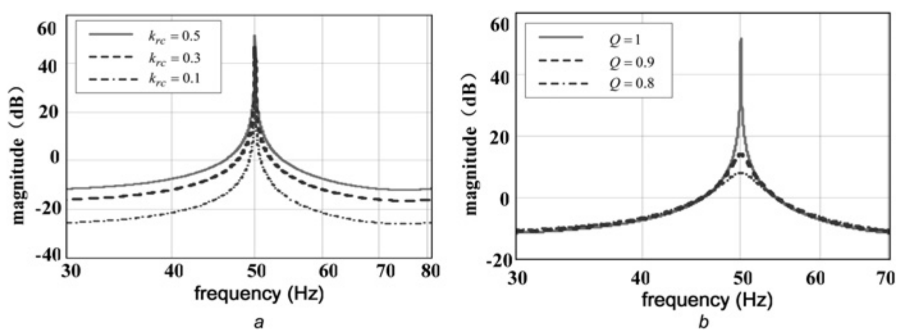

Fig. 8 *Bode plot of harmonic compensator $G_{rc}(s)$ with different parameters k_{rc} and Q*

a $G_{\rm rc}(s)$ with different $k_{\rm rc}$ and $Q = 1$
b $G_{\rm rc}(s)$ with different Q and $k_{\rm rc} = 0.5$

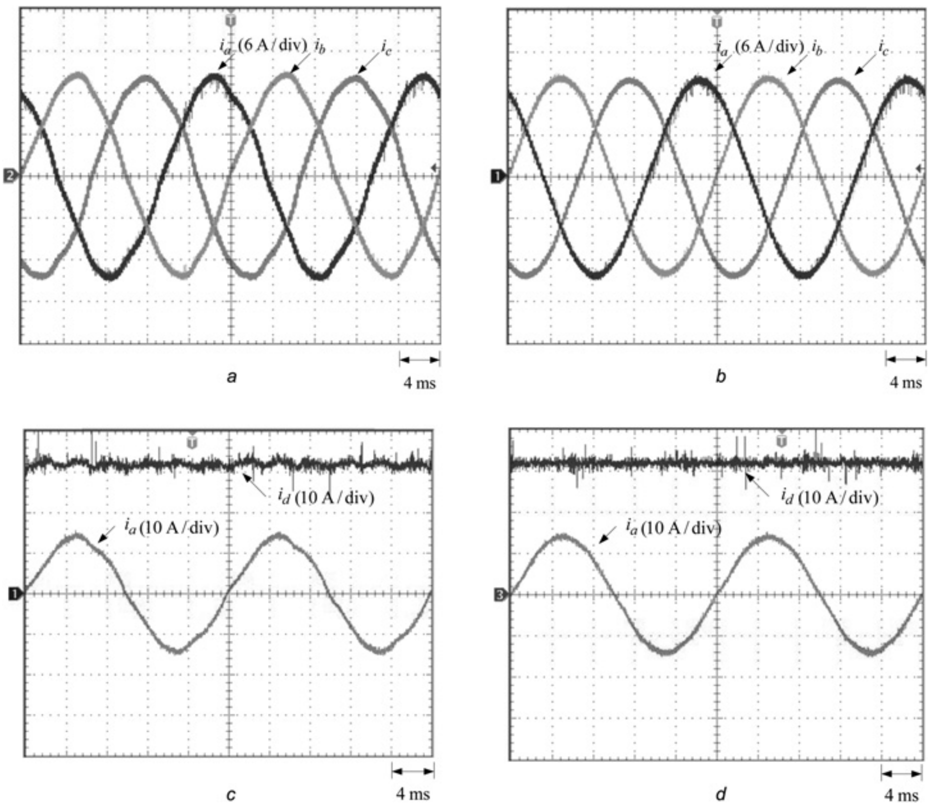

Fig. 10 *Performance of VSI with and without RC harmonic compensator in steady state*

a Three-phase output currents without RC harmonic compensator
b Three-phase output currents with RC harmonic compensator
c Output current i_a and transformed current i_d without RC harmonic compensator
d Output current i_a and transformed current i_d with RC harmonic compensator

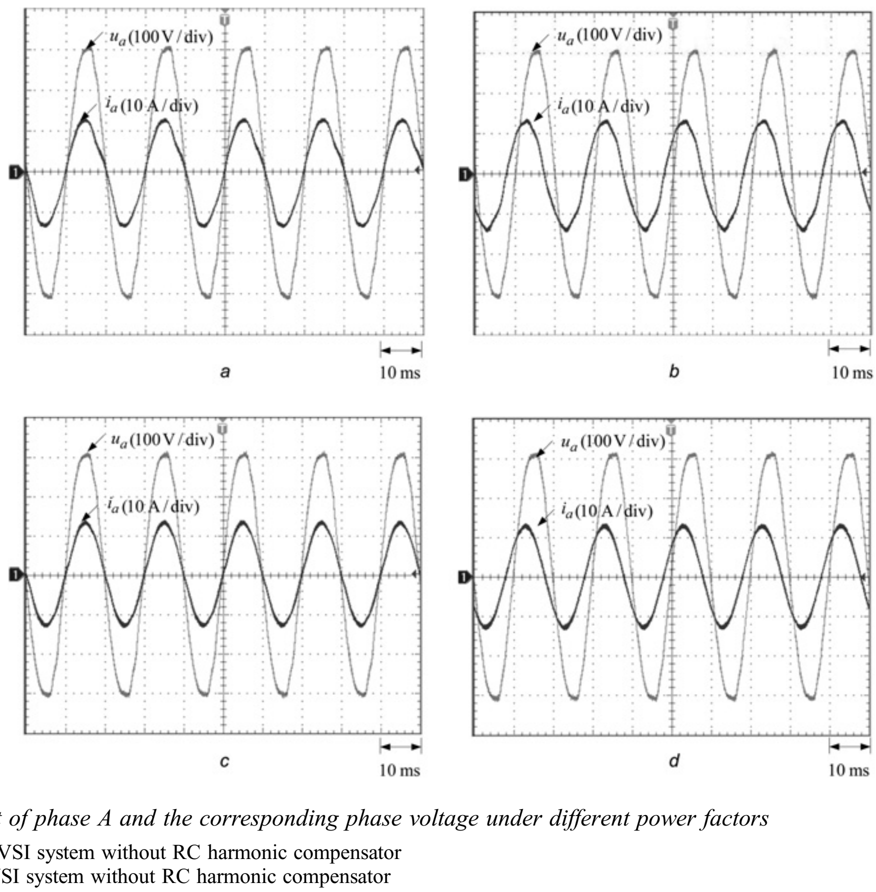

Fig. 11 *Output current of phase A and the corresponding phase voltage under different power factors*

a Unit power factor of the VSI system without RC harmonic compensator
b 0.8 power factor of the VSI system without RC harmonic compensator
c Unit power factor of the VSI system with RC harmonic compensator
d 0.8 power factor of the VSI system with RC harmonic compensator

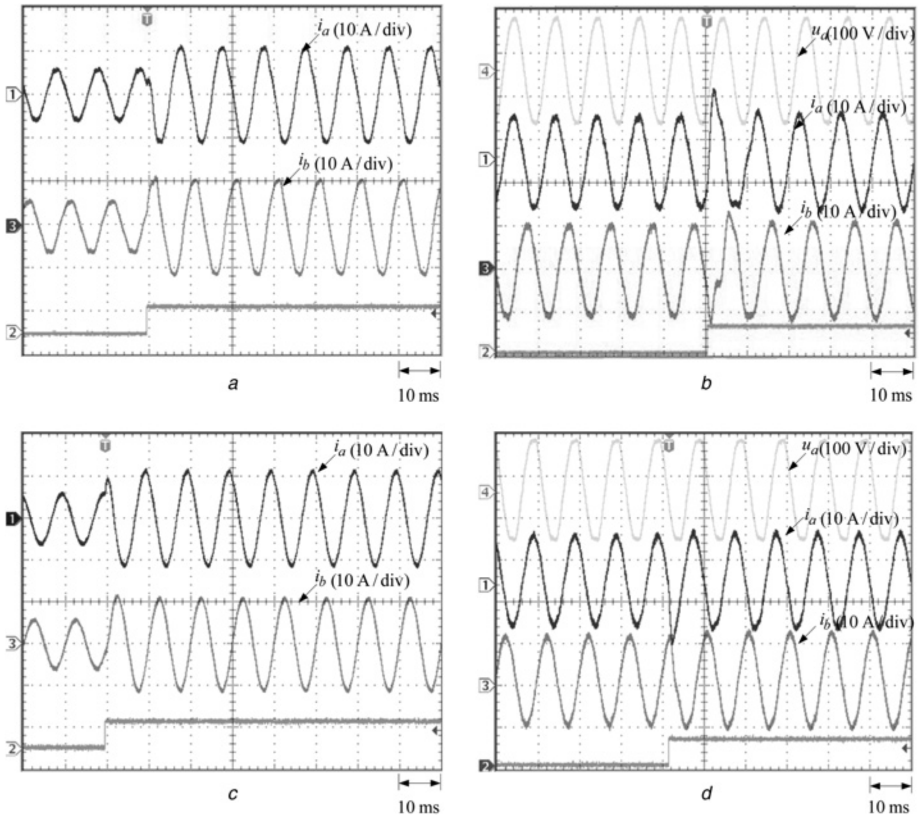

a b c d

Fig. 12 *Experimental transient response against step changes*

a Step change in amplitude with the current of phase A and phase B without RC compensator
b Change in power factor with current of phase A, phase B and the grid voltage of phase A without RC compensator
c Step change in amplitude for the current of phase A and phase B with RC compensator
d Change in power factor with current of phase A, phase B and the grid voltage of phase A with RC compensator

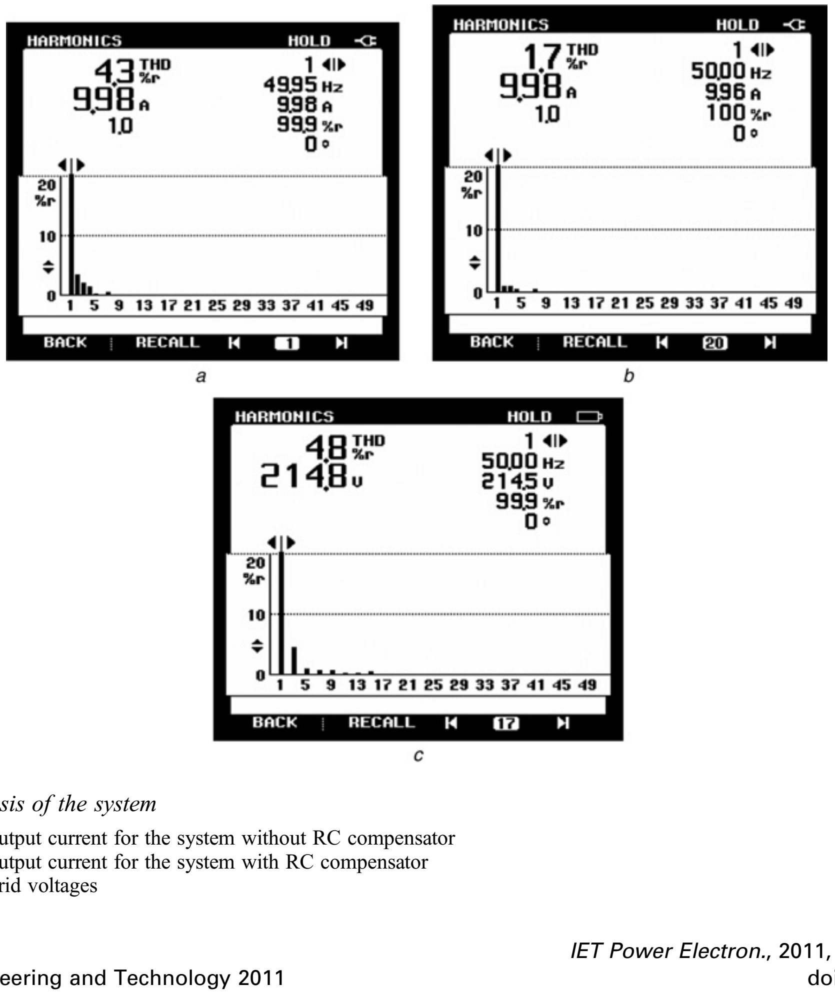

a b c

Fig. 13 *Harmonics analysis of the system*

a Harmonics analysis of the output current for the system without RC compensator
b Harmonics analysis of the output current for the system with RC compensator
c Harmonics analysis of the grid voltages

doi: 10.1049/iet-pel.2010.0231

compensator. When only the PI controller is used, it can be seen from Fig. 10*c* that the current distortion of single phase will mainly cause sixth harmonics of the output currents in $d-q$ reference frame. When RC harmonic compensator is implemented, the harmonics in i_a and i_d are well compensated as shown.

Fig. 11 shows the waveforms of the inverter output currents and the corresponding grid voltages, at different output power factors, for the systems with and without the RC compensator. In Figs. 11*a* and *c*, the three-phase VSI systems are at a unity power factor. Since that the power factor of the hybrid system can be conveniently controlled in SRF, the three-phase VSI systems with leading power factor of 0.8 are shown in Figs. 11*b* and *d*. It is worth noticing that although harmonics distortion in grid voltage is 4.8%, the inverter output currents are almost sinusoidal with a THD of 1.8% in these two cases with the RC compensator.

Fig. 12 shows the experimental transients of the inverter output currents facing the step changes of the references, with and without the RC compensator. Figs. 12*a* and *c* show that the references of the inverter are changed in amplitude, and Figs. 12*b* and *d* present the inverter are against a change in power factor from unit to 0.8, by setting the reference in *q* frame unequal to zero. As can be seen that with the RC compensator, although distortion and overshoot of currents exist in the dynamic response, the THD of the output currents is less than 2.5% in the both situations when the dynamic process finishes.

Fig. 13 shows the harmonics analysis of the system by Fluke 43B power harmonic analyser. For comparison, Figs. 13*a* and *b* present the harmonic analysis of the output current with and without the RC compensator, and Fig. 13*c* is the harmonic analysis of the grid-side voltages.

6 Conclusions

This paper presents a hybrid controlled three-phase grid-connected inverter in synchronous reference ($d-q$) frame. A systematic theoretical analysis considering system stability constraints of the hybrid controlled system in $d-q$ frame, the steady-state and dynamic response, and a set of design tradeoffs relating parameters selection in the hybrid controller, are further discussed from the frequency view point. Moreover, this paper also reveals the different roles of the PI controller and repetitive controller in $d-q$ frame during regulation procedures of the system. Based on this analysis, a design procedure is formulated and experiments are carried out. The results show that with the RC harmonic compensator, the three-phase VSI system can be effectively immune to the grid voltage distortions and achieve very low THD of output currents. The experimental results also reveal that the hybrid controller makes the system achieve satisfactory dynamic performance, which also can improve the slow system dynamic response of the repetitive controller designed in static reference frame.

7 Acknowledgment

This work was supported by National Nature Science Foundation of China (grant no. 50807005).

8 References

1 Carrasco, J., Franquelo, L., Bialasiewicz, J., *et al.*: 'Power-electronic systems for the grid integration of renewable energy sources: A survey', *IEEE Trans. Ind. Electron.*, 2006, **53**, (3), pp. 1002–1016
2 Ibrahim Mohamed, Y.A., El-Saadany, E.F.: 'A control scheme for PWM voltage-source distributed-generation inverters for fast load-voltage regulation and effective mitigation of unbalanced voltage disturbances', *IEEE Trans. Ind. Electron.*, 2008, **55**, (5), pp. 2072–2084
3 Blaabjerg, F., Chen, Z., Kjaer, S.: 'Power electronics as efficient interface in dispersed power generation systems', *IEEE Trans. Power Electron.*, 2004, **19**, (5), pp. 1184–1194
4 IEEE15471: 'IEEE standard for interconnecting distributed resources with electric power systems', 2005
5 Gonzalez, R., Gubia, E., Lopez, J., Marroyo, L.: 'Transformerless single-phase multilevel-based photovoltaic inverter', *IEEE Trans. Ind. Electron.*, 2008, **55**, (7), pp. 2694–2702
6 Figueres, E., Garcera, G., Sandia, J., Gonzalez-Espin, F., Rubio, J.: 'Sensitivity study of the dynamics of three-phase photovoltaic inverters with an LCL grid filter', *IEEE Trans. Ind. Electron.*, 2009, **56**, (3), pp. 706–717
7 Espí Huerta, J., Castelló-Moreno, J., Fischer, J.R., García-Gil, R.: 'A synchronous reference frame robust predictive current control for three-phase grid-connected inverters', *IEEE Trans. Ind. Electron.*, 2010, **57**, (3), pp. 954–962
8 Dahono, P.A.: 'New hysteresis current controller for single-phase full-bridge inverters', *IET Power Electron.*, 2009, **2**, (5), pp. 585–594
9 Mattavelli, P.: 'A closed-loop selective harmonic compensation for active filters', *IEEE Trans. Ind. Appl.*, 2001, **37**, (1), pp. 81–89
10 Liserre, M., Teodorescu, R., Blaabjerg, F.: 'Multiple harmonics control for three-phase grid converter systems with the use of PI-RES current controller in a rotating frame', *IEEE Trans. Power. Electron.*, 2006, **21**, (3), pp. 836–841
11 Zmood, D., Holmes, D.G.: 'Stationary frame current regulation of PWM inverters with zero steady-state error', *IEEE Trans. Power Electron.*, 2003, **18**, (3), pp. 814–822
12 Chen, S., Lai, Y.M., Tan, S.-C., Tse, C.K.: 'Analysis and design of repetitive controller for harmonic elimination in PWM voltage source inverter systems', *IET Power Electron.*, 2008, **1**, (4), pp. 497–506
13 Escobar, G., Valdez, A.A., Leyva-Ramos, J.: 'Repetitive-based controller for a UPS inverter to compensate unbalance and harmonic distortion', *IEEE. Trans. Ind. Electron.*, 2007, **54**, (1), pp. 504–510
14 Zhang, K., Kang, Y., Xiong, J., Chen, J.: 'Direct repetitive control of SPWM inverter for UPS purpose', *IEEE Trans. Power. Electron.*, 2003, **1**, (3), pp. 784–792
15 Francis, B.A., Wonham, W.M.: 'The internal model principle for linear multivariable regulators', *Appl. Math.*, 1975, **2**, pp. 170–194
16 Zhou, L., Wu, M., She, J.: 'Design of observer-based robust repetitive-control system'. Proc. Int. Conf. Robotics and Biomimetics, December 2009, pp. 2079–2084
17 Zhang, B., Wang, D., Zhou, K.L., Wang, Y.: 'Linear phase lead compensation repetitive control of a CVCF PWM inverter', *IEEE Trans. Ind. Electron.*, 2008, **55**, (4), pp. 1595–1602
18 Chen, S., Lai, Y.M., Tan, S.-C., Tse, C.K.: 'Fast response low harmonic distortion control scheme for voltage source inverters', *IET Power Electron.*, 2009, **2**, (5), pp. 574–584
19 Zhou, K.L., Kay-Soon, L., Wang, D., Fang, L., Zhang, B., Wang, Y.: 'Zero-phase odd-harmonic repetitive controller for a single-phase PWM inverter', *IEEE. Trans. Power. Electron.*, 2006, **21**, (1), pp. 193–196
20 Zhou, K.L., Wang, D., Zhang, B., Wang, Y.: 'Plug-in dual-mode-structure repetitive controller for CVCF PWM inverters', *IEEE. Trans. Ind. Electron.*, 2009, **56**, (3), pp. 784–791
21 Lascu, C., Asiminoaei, L., Boldea, I., Blaabjerg, F.: 'Frequency response analysis of current controllers for selective harmonic compensation in active power filters', *IEEE. Trans. Ind. Electron.*, 2009, **56**, (2), pp. 337–347
22 Lascu, C., Asiminoaei, L., Boldea, I., Blaabjerg, F.: 'High performance current controller for selective harmonic compensation in active power filters', *IEEE. Trans. Ind. Electron.*, 2007, **22**, (5), pp. 1826–1835